Chapter 8 -- Configuration Flexibility and Robustness

8.1   Introduction

In order to achieve the scientific goals of the NCSX mission, the NCSX device must be capable of supporting a range of variations in plasma configuration about the reference baseline equilibrium. In the following Sections we present a number of numerical calculations which demonstrate the ability of the CDR coilset, described in detail in both Chapter 2 and in the Engineering Design Document, to provide this wide range of configurations. Many of the calculations are similar to those presented at the Physics Validation Review (PVR) in March 2001 and presented in Chapter 9 of the Physics Validation Report. The PVR flexibility calculations used the M1017 modular coilset comprising 4 independent coil types in each of the 3 field periods, a pure 1/R auxiliary toroidal field coil system modeled by a single vertical wire filament on the machine centerline (R=0), and an idealized axisymmetric poloidal field coil system modeled as 4 independent axisymmetric multipoles (Dipole, Quadrapole, Hexapole and Octapole). The improved CDR modular coilset (designated M45) has 3 independent modular coil types per period rather than four. The CDR poloidal field coilset has 6 independent coil groups, two of which provide ohmic magnetic fields and the remaining four provide high quality axisymmetric multipole fields. In addition, the CDR toroidal field coilset comprises 18 planar TF coils which provide an excellent 1/R toroidal field distribution.

Figure 8-1 shows a top view of the modular coil set M45 used for the flexibility and robustness studies presented here. There are 6 coils in each of the three periods of the machine. Stellarator symmetry implies that within any given period only 3 coil currents are independent. The independent coils are labeled "1", "2"and "3". Stellarator-symmetric partners are labeled with prime superscripts. The same numbering convention will be used to identify the coils when presenting coil current solutions in our flexibility studies.
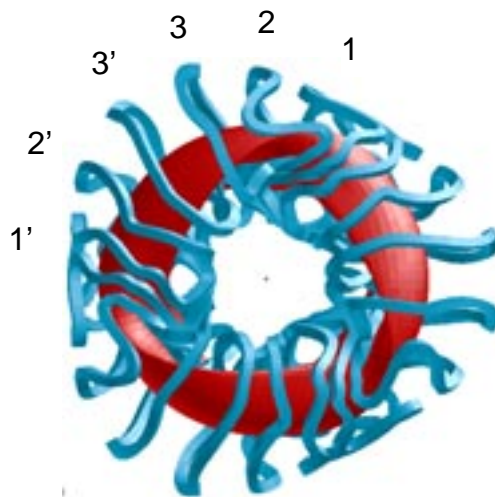
Figure 8-1. Modular coilset M45 used for flexibility and robustness studies. Integers "1", "2" and "3" label the three coils within each period whose coil currents are allowed to vary independently of one another. Coil k' is the stellarator symmetric partner of coil k

The three modular coil currents are allowed to vary independently; thus the mean (toroidally averaged) toroidal magnetic field at a given radius will also vary. For systematic experiments it is advantageous to separate the provision of external transform by 3D shaping from provision by changes in the average toroidal field. In principle, the average toroidal field can be constrained to be a constant value by varying only two linear combinations of the three modular coil currents. However this leads to a considerable reduction in the flexibility of NCSX to control the external transform. To avoid such a reduction in flexibility NCSX includes an auxiliary TF coil system where the TF coil current is allowed to vary together with the three modular coil currents in such a way that the mean TF field remains constant. The TF coil system is comprised of 18 coils connected in series, capable of providing 0.5T at the radius R = 1.4 m.
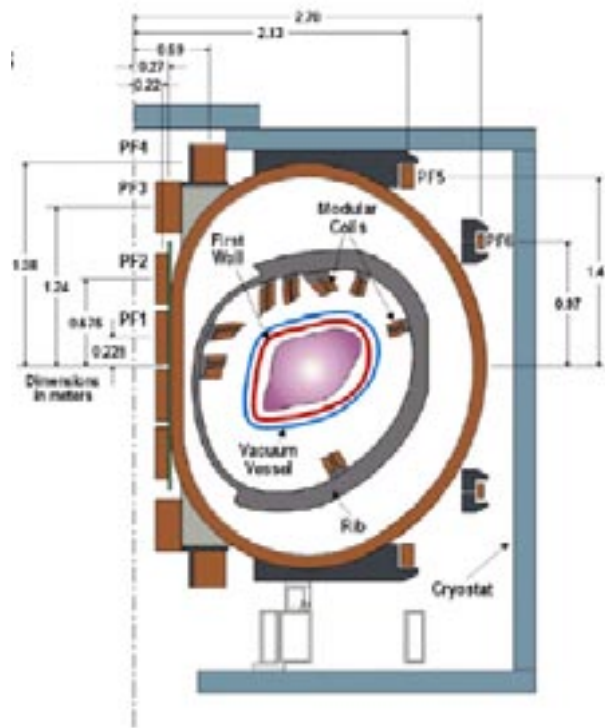
Figure 8-2. Poloidal field coils labelled PF1 – 6 provide additional flexibility for the accomplishment of the physics mission

A system of six axisymmetric poloidal field currents is included for additional flexibility (see Figure 8.2). Coil PF6 is positioned to give a high quality dipole (vertical) field in the plasma region. PF5 is positioned so that, in combination with PF6, a high quality quadrupole field is produced. Coils PF4 and PF3 produce, in combination with PF5 and 6, hexapole and octapole fields, respectively. Coils PF1 and PF2 are the primary ohmic heating coils and play no role in the flexibility calculations presented in this Chapter.

Table 8.1 shows coil current limits for each of the independent coil systems (see Appendix 1 of the Engineering Design Document). Plasma configurations are required to have coil currents that lie within these limits.

M 1 [kA-turns]	M 2 [kA-turns]	M 3 [kA-turns]	TF [kA-turns]	PF3 [kA-turns]	PF4 [kA-turns]	PF5 [kA-turns]	PF6 [kA-turns]
864.0	864.0	864.0	±194.	±1739.0	±1397.0	±182.0	±73.0

Table 8-1. Coil current limits [kA-turns] per coil for each of the coil systems. M = Modular, TF = Toroidal Field, PF = Poloidal Field. Plasma configurations produced in the flexibility studies require coil currents within the given limits

The primary computational tool for the flexibility studies is STELLOPT, a VMEC-based free-boundary optimizer which varies coil currents to target configurations with specific physics properties, such as stability to kink and ballooning modes and good quasi-axisymmetry (QA). Essential code modules within STELLOPT include an equilibrium solver (VMEC[1]), stability analysis codes (TERPSICHORE[2] for kink modes, COBRA[3] for ballooning modes), and a QA analyser. For the calculations presented here, the QA-ness measure targeted in STELLOPT is either $\chi^2_{Bmn} = \Sigma' B^2_{mn}/B^2_{00}$ where the B_{mn} are Fourier components of the magnetic field analysed on the s=0.3, s=0.5, and s=0.8 magnetic surfaces evaluated in Boozer magnetic coordinates, with the summation taken over modes with n>0, or ε_h the effective helical ripple calculated by the NEO[4] code module. The targeted stability measures are, $\chi^2_K = \lambda_K^2{}_{n=1} + \lambda_K^2{}_{n=0}$ (the square of the unstable eigenvalue of the dominant kink instability for the n=1 and n=0 kink families), and $\chi^2_B = \Sigma\lambda_B^2$ (the sum of squares of the maximum ballooning eigenvalue on any of the 49 magnetic surfaces used in the calculation of VMEC equilibria). Optimized equilibria are further constrained to be tangent at some point to the plasma-facing-component first wall.

The M45 coil geometry was determined (see Chapter 2) with the requirement that coil currents can be found which support a free-boundary equilibrium that reproduces the physics properties of the reference li383 S3 plasma configuration (I_p = 174 kA, B_T = 1.7 T at R = 1.4 m, stable to kink and ballooning modes at β > 4.2%, good quasi-axisymmetry with effective helical ripple $\varepsilon_h \sim$ 0.5% at s=0.5). The reference configuration assumes bootstrap consistency between the current and pressure profiles. The reference profiles and reference S3 plasma shape are shown in Figures 8-3 and 8-4. Coil currents that produce S3 are presented in Table 8-2. A summary of the shape and physics parameters for the kink and ballooning stable reference S3 state is given in Table 8-3.

M 1 [kA-turns]	M 2 [kA-turns]	M 3 [kA-turns]	TF [kA-turns]	PF3 [kA-turns]	PF4 [kA-turns]	PF5 [kA-turns]	PF6 [kA-turns]
694.2	654.6	551.1	27.8	1524.2	1180.0	95.2	-2.3

Table 8-2. Coil currents for the reference S3 state using the plasma profiles shown in Figure 8-2. I_p = -174 kA, B_T = 1.7 T, β = 4.1%. Currents in ohmic coils PF1 and PF2 are zero.
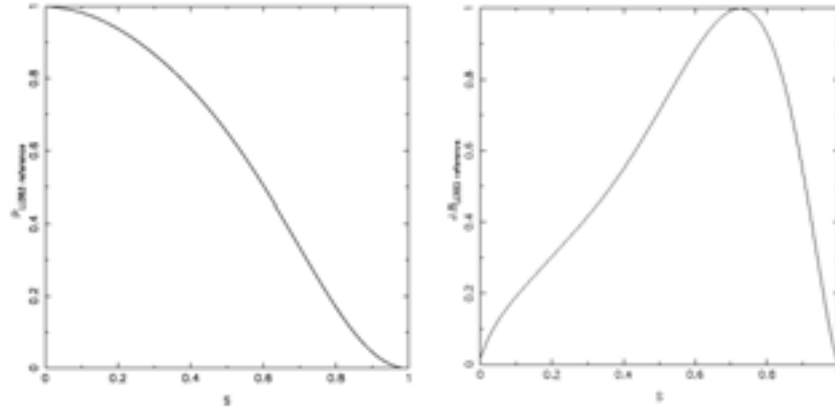
Figure 8-3. Baseline 'reference' current (J.B) and pressure (p) profiles as a function of normalized toroidal flux, s
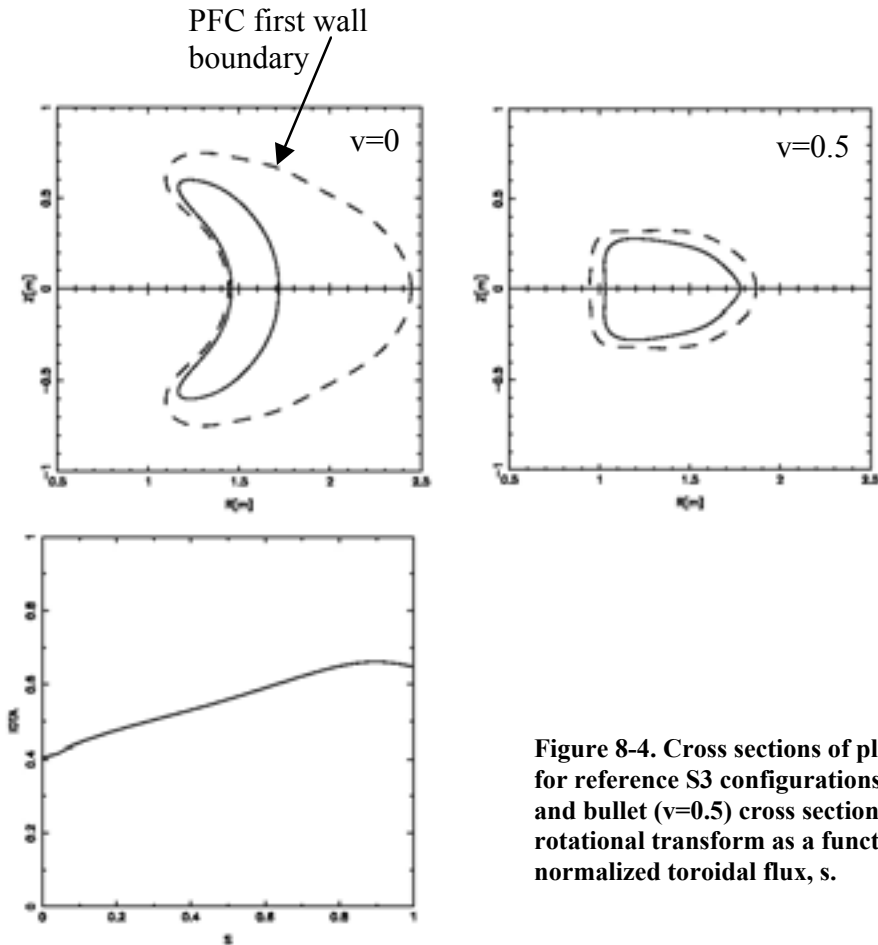
Figure 8-4. Cross sections of plasma shape for reference S3 configurations at bean (v=0) and bullet (v=0.5) cross sections. Also rotational transform as a function of normalized toroidal flux, s.

I_p [kA]	B_T [T]	R [m]	A	β [%]	$\varepsilon_{eff}(s=0.5)$ [%]	$\iota(0)$	$\iota(1)$	ι_{max}
–174.	1.70	1.40	4.37	4.1	0.45	0.40	0.65	0.66

Table 8-3. Shape and physics parameters for kink and ballooning stable reference S3 plasma configuration.

The reference S3 configuration defines a single point in the operating space of NCSX. In the following subsections we address the following questions on robustness and performance: Using the M45 coilset

- How does the plasma performance change as currents and profiles are changed from the reference?
- Is the operating space for configurations with adequate performance characteristics wide enough to allow fulfillment of the NCSX mission?
- Can the designed coils produce the magnetic fields required to support this range of plasma configurations?

8.2 Robustness of Plasma Performance w.r.t. Change in Coil Current

In this Section we investigate the robustness of plasma performance to changes in individual coil currents using fixed plasma profiles. Whereas in later Sections we use STELLOPT to find coil currents that support configurations with targeted physics properties, allowing several coil currents to vary, here we investigate whether plasma shape and performance are sensitive (unstable) or insensitive (stable) to small changes in coil current. Companion calculations were presented in the PVR document where the sensitivity of plasma shape and performance to changes in pressure and current profile shape, net plasma toroidal current and plasma beta were investigated using coil currents fixed at values corresponding to the reference S3 state.

Eight perturbations of the S3 configuration were induced by separately incrementing each of the coil currents required to produce S3 (the currents shown in Table 8-2) by 5% of the maximum current allowed for that coil. A ninth perturbation was defined by incrementing the plasma current by 5% of the reference S3 value. Free boundary equilibria were calculated for each of these coil current perturbations at fixed toroidal flux, and the change in selected plasma parameters noted in Table 8-4.

The small changes in $R_{max/min}$ and Z_{max} at any toroidal angle which result from perturbing the coil currents imply that the plasma shape is robust with respect to the coil current changes. The neoclassical transport measure, ε_{eff}, is also well-preserved. In some cases a change in stability of either kink or ballooning modes is observed. The reason for this change in stability is the following: The optimizer which produced the reference configuration uses a heavyside cost function measure of stability with $\chi^2_K = \lambda^2_K > 0$ for unstable kink eigenvalues, λ_K, while $\chi^2_K = 0$ for a kink stable configuration. Since the total χ^2 summed over all physics measures is minimized, optimum configurations are <u>marginally stable</u> to kink and ballooning modes.

Perturbations of optimum configurations produced in this way are typically destabilized. As will be seen in later Sections, the heavyside cost function feature of STELLOPT can be exploited to design experiments to test 3D effects on β- limits at low beta. The small changes in shape and parameters produced by arbitrary coil current perturbations of the optimized S3 configuration imply nothing as to the ability to derive configurations with very different properties to S3. We will see in later Sections that NCSX flexibility is considerable if the correct coil current perturbations are used.

PERTURBED CIRCUIT	M1	M2	M3	TF	PF3	PF4	PF5	PF6	I_P
ΔI[kA-turns]	+43.2	+43.2	+43.2	+9.7	+87.0	+69.9	+9.1	+3.7	+8.7
ΔR_{max}[cm]	-0.3	-0.5	-2.2	-1.4	-0.0	-0.2	-0.6	-0.1	-0.7
ΔR_{min}[cm]	+0.2	+0.3	+0.3	+0.8	-0.0	-0.2	-0.2	-0.0	-0.1
ΔZ_{max}[cm]	-1.5	-0.7	+0.0	-1.4	-0.1	-0.1	+0.1	+0.1	-0.2
ΔA	+0.05	+0.05	+0.05	+0.04	+0.00	-0.00	-0.01	-0.00	+0.00
$\Delta \beta$ [%]	-0.18	-0.47	-0.19	-0.13	-0.00	-0.01	-0.01	-0.00	+0.00
$\Delta\iota(0)$	+0.005	+0.005	-0.004	-0.011	+0.001	+0.002	+0.002	+0.000	-0.000
$\Delta\iota(1)$	+0.005	-0.001	-0.008	-0.016	+0.000	-0.001	-0.004	-0.001	+0.019
ΔRB_T[T-m]	+0.05	+0.05	+0.05	+0.03	+0.00	+0.00	+0.00	-0.001	+0.00
ΔKink $_{(n=0)}$	S→S↓	S→S	S→U	S→U	S→S	S→S	S→S	S→S	S→U
ΔKink $_{(n=1)}$	S→S↓	S→S	S→U	S→U	S→S	S→S	S→S	S→S	S→U
ΔBall $_{(n=\infty)}$	S→U	S→S↑	S→S↓	S→S↑	S→S	S→S	S→S	S→S	S→U
$\Delta\varepsilon_{eff}$[%]	+0.08	-0.02	+0.12	-0.02	-0.01	-0.02	-0.03	-0.01	-0.01

Table 8-4. Effect on plasma parameters of perturbing the S3 state by incrementing modular coil current (M), toroidal field coil current (TF) , poloidal field coil current (PF) and plasma current (I_p) by 5% of the max allowed current. $\Delta R_{max/min}$ is change in max/min plasma radius at any toroidal angle; ΔZ_{max} is change in max plasma height at v=0 (bean) cross section; ΔA is change in plasma aspect ratio; $\Delta\beta$ is change in plasma beta; $\Delta\iota(0)$ and $\Delta\iota(1)$ are change in axis and edge values of the total rotational transform; ΔRB_T is change in radius times toroidal magnetic field, evaluated at R=1.4m; ΔKink $_{(n=0,1)}$ refers to change in stability of n=0 and n=1 family of kink modes – S denotes stable, S↑ denotes an increase in stability margin compared with the reference case, and S↓ denotes a decrease in stability margin. U denotes unstable; ΔBall $_{(n=\infty)}$ refers to change in stability of ballooning modes; $\Delta\varepsilon_{eff}$ is change in effective helical ripple evalueated at the s=0.5 surface.

In the following Sections, we investigate the performance of plasmas whose profiles and/or beta and net toroidal current differ from their reference forms and/or values. Coil currents are allowed to vary in such a way that χ^2_{Bmn} is minimized while kink and ballooning stability are enforced. Plasmas are further constrained to be limited by the first wall boundary. We will show that stable plasmas with good quasi-axisymmetry can be obtained for a wide range of assumed plasma conditions.

8.3 Robustness of Performance as β and I_p are Varied

In Chapter 9, discharge simulations are presented as a sequence of free-boundary equilibria corresponding to the "evolution" of an NCSX plasma from a particular S1 state where $\beta = 0.0\%$ to a final S3 state where $\beta > 4\%$. Pressure profile evolution is consistent with a 1-D transport model. The evolution from initial to final states can be represented as a curve on an I_p - β plane. Each point on the curve is associated with a particular profile of plasma current and pressure.

In this Section, we explore the performance of NCSX plasmas for a wide range of values of β and I_p using fixed reference profiles; the S3 profiles of current and pressure shown in Figure 8-3. In each case coil currents were varied to produce shape deformations of the plasma that lead to the minimization of a linear combination of χ^2_{Bmn} and the (square of the) growth rates for kink and ballooning modes. The average toroidal field was constrained to be constant, with $B_T = 1.7$ T at R=1.4 m. Plasmas were further constrained to be limited by the first wall boundary.

Results are presented in Table 8-5. In each block is listed the kink and ballooning mode stability characteristics of the optimized configuration, as well as the effective helical ripple strength, $\varepsilon_h[\%]$, evaluated on the s=0.3, s=0.5, and s=0.8 magnetic surfaces. Stable free-boundary equilibria were found for nearly every case in the calculated I_p - β plane. All equilibria were stable to kink modes; nearly all equilibria were stable to ballooning modes. For $I_p = -174$ kA the free-boundary equilibrium with $\beta = 5.0\%$ was stable to both ballooning and kink modes. This β value is substantially higher than the reference li383 fixed boundary β-limit. (A full exploration of the maximum β-limit using the M45 coils has not yet been made; however, a kink stable configuration was found with $\beta = 6.0\%$ and $\varepsilon_h = 0.8\%$ at s = 0.5 using the standard (unoptimized) S3 profiles. Ballooning modes for this $\beta = 6\%$ configuration were unstable on two adjacent magnetic surfaces near the edge of the plasma). Two cases in Table 8-5 were unstable to ballooning modes. These cases (orange-filled boxes) are $I_p = 0$ kA, $\beta = 3.0\%$ and $I_p = 0$ kA, $\beta = 4.0\%$. With regard to QA-ness, $\varepsilon_h < 0.5\%$ at s=0.5, typically, and ε_h never exceeds 1.0% at s = 0.5. As discussed in Chapter 7, it is expected that for this magnitude of ripple amplitude, and with standard conditions of plasma temperature and density, the helical ripple transport will be small compared with axisymmetric neoclassical transport.

Using reference profiles, we conclude there is a substantial region of stability with good QA-ness in the I_p - β plane. The results here and in later Sections are very similar to those presented at the PVR.

β[%] →	0.0	1.0	2.0	3.0	4.0	5.0
Ip[kA]						
0	Kink: N/A Balloon: N/A ε_h [%] = 0.33 0.79 1.96 **S1**	Kink: N/A Balloon: S ε_h [%] = 0.37 0.89 2.02	Kink: N/A Balloon: S ε_h [%] = 0.37 0.14 1.85	Kink: N/A **Balloon:** **U**	Kink: N/A **Balloon:** **U**	C A S E S
-44.	Kink: S Balloon: N/A ε_h [%] = 0.30 0.77 1.79	Kink: S Balloon: S ε_h [%] = 0.29 0.68 1.52	Kink: S Balloon: S ε_h [%] = 0.31 0.67 1.58	Kink: S Balloon: S ε_h [%] = 0.30 0.61 1.43	Kink: S Balloon: S ε_h [%] = 0.37 0.71 1.63	N O T
-87.5	Kink: S Balloon: N/A ε_h [%] = 0.27 0.71 1.64	Kink: S Balloon: S ε_h [%] = 0.28 0.65 1.51	Kink: S Balloon: S ε_h [%] = 0.26 0.51 1.22	Kink: S Balloon: S ε_h [%] = 0.39 0.72 1.58	Kink: S Balloon: S ε_h [%] = 0.31 0.60 1.60	S T U
-131.	Kink: S Balloon: N/A ε_h [%] = 0.23 0.52 1.33	Kink: S Balloon: S ε_h [%] = 0.25 0.46 1.06	Kink: S Balloon: S ε_h [%] = 0.23 0.42 1.06	Kink: S Balloon: S ε_h [%] = 0.29 0.41 0.95	Kink: S Balloon: S ε_h [%] = 0.23 0.45 1.23	D I E D
-174	Kink: S Balloon: N/A ε_h [%] = 0.19 0.37 **S2** 0.93	Kink: S Balloon: S ε_h [%] = 0.21 0.39 0.95	Kink: S Balloon: S ε_h [%] = 0.18 0.36 0.82	Kink: S Balloon: S ε_h [%] = 0.19 0.40 1.04	Kink: S Balloon: S ε_h [%] = 0.21 **S3** 0.45 1.15	Kink: S Balloon: S ε_h [%] = 0.56 0.92 2.15

Table 8-5. NCSX plasma performance for a wide range of β, I_p values. In all but the two cases shown in the orange blocks, optimized configurations were found to be stable (S) to kink and ballooning modes with good quasi-axisymmetry. Only I_p = 0 kA, β = 3% and I_p = 0 kA, β = 4% were unstable (U) - to ballooning modes. The effective helical ripple strength, ε_h, is tabulated for the s=0.3, s=0.5, and s=0.8 magnetic surfaces. It is small over the entire range of the Table. A stable configuration was obtained at I_p = -174 kA, β = 5%.

The range of variation for the coil currents which produce the optimized configurations of the I_p - β scan is presented in Table 8-6. For the modular coil currents the variation is less than 10% from the nominal S3 currents (Table 8-2). The variation in poloidal field coil current is ~100%. Plots of coil current versus beta, as a fraction of allowed current, are shown in Figure 8-5 for the diagonal sequence $I_p \propto \beta$ connecting the vacuum state, S1, and the reference full current, high beta state, S3. Coil currents for this sequence, as well as for all cases shown in Table 8-5 are within the allowables.

An overlay of plasma boundaries and calculated iota profiles for a subset of stable equilibria from the I_p - β scan are presented in Figure 8-6. A wide range of plasma boundary shapes and iota profiles is seen, including a substantial variation in magnetic shear, $d\iota/ds$. This data shows the possibility of designing experiments to investigate shear stabilization of neoclassical tearing modes. Later, in Section 8.6, we show how the ability to control $\iota(s)$ at fixed I_p and β using the external magnetic fields allows the design of experiments to investigate 3D shape stabilization of external kink modes.

ΔI_{M1} [kA-turns]	ΔI_{M2} [kA-turns]	ΔI_{M3} [kA-turns]	ΔI_{TF} [kA-turns]	ΔI_{PF3} [kA-turns]	ΔI_{PF4} [kA-turns]	ΔI_{PF5} [kA-turns]	ΔI_{PF6} [kA-turns]
+52.	+41.	+46.	+31.	+0.	+0.	+78.	+28.
-38.	-12.	-27.	-46.	-1691.	-1627.	-222.	-36.

Table 8-6. Coil current variation for the Ip - β scan results. In each column is shown the max +/- variation in the current for coil "k" compared with the current required to support the S3 state.
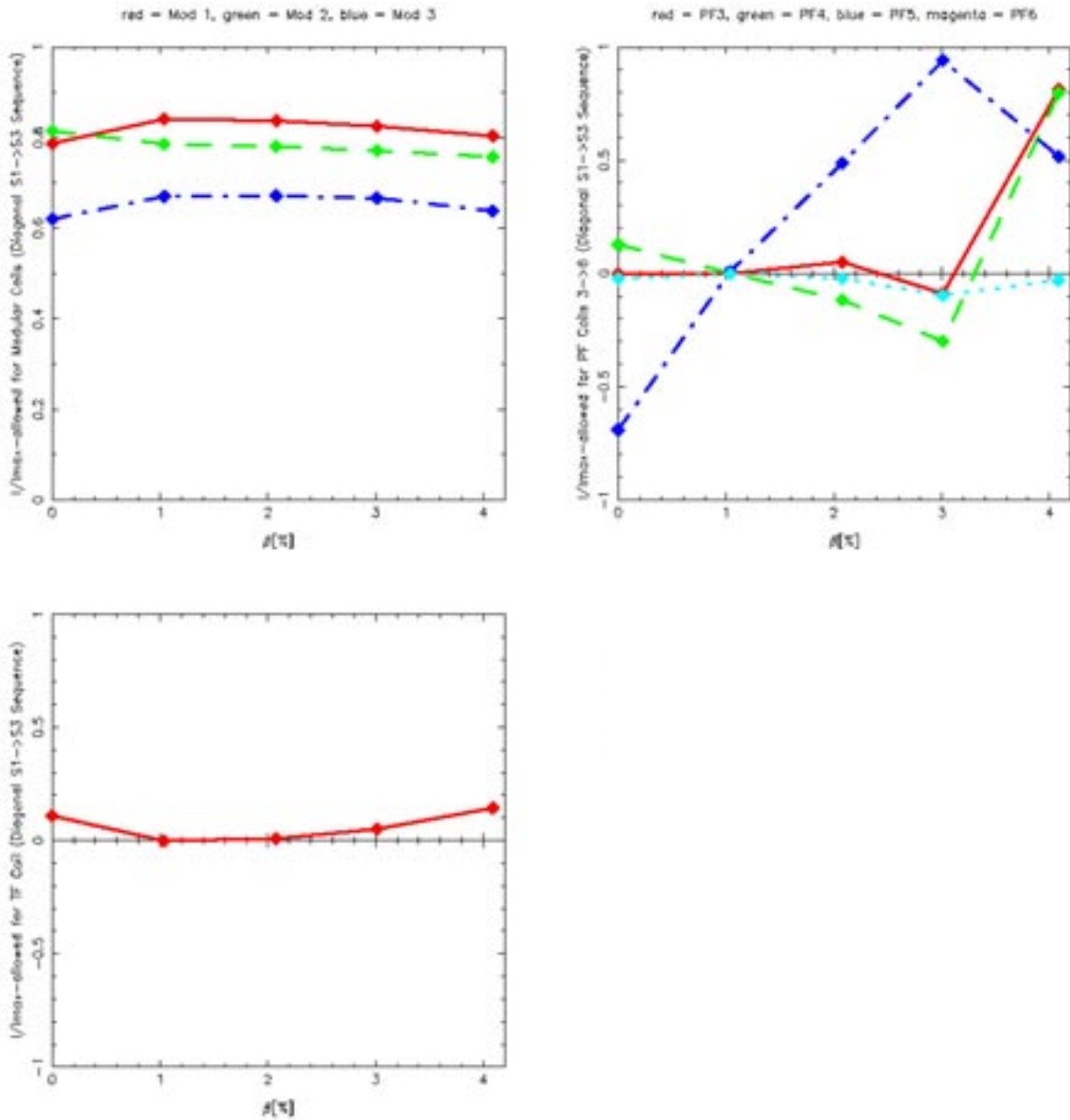
Figure 8-5. Coil currents as fraction of allowable current per coil for the sequence $I_p \propto \beta$.
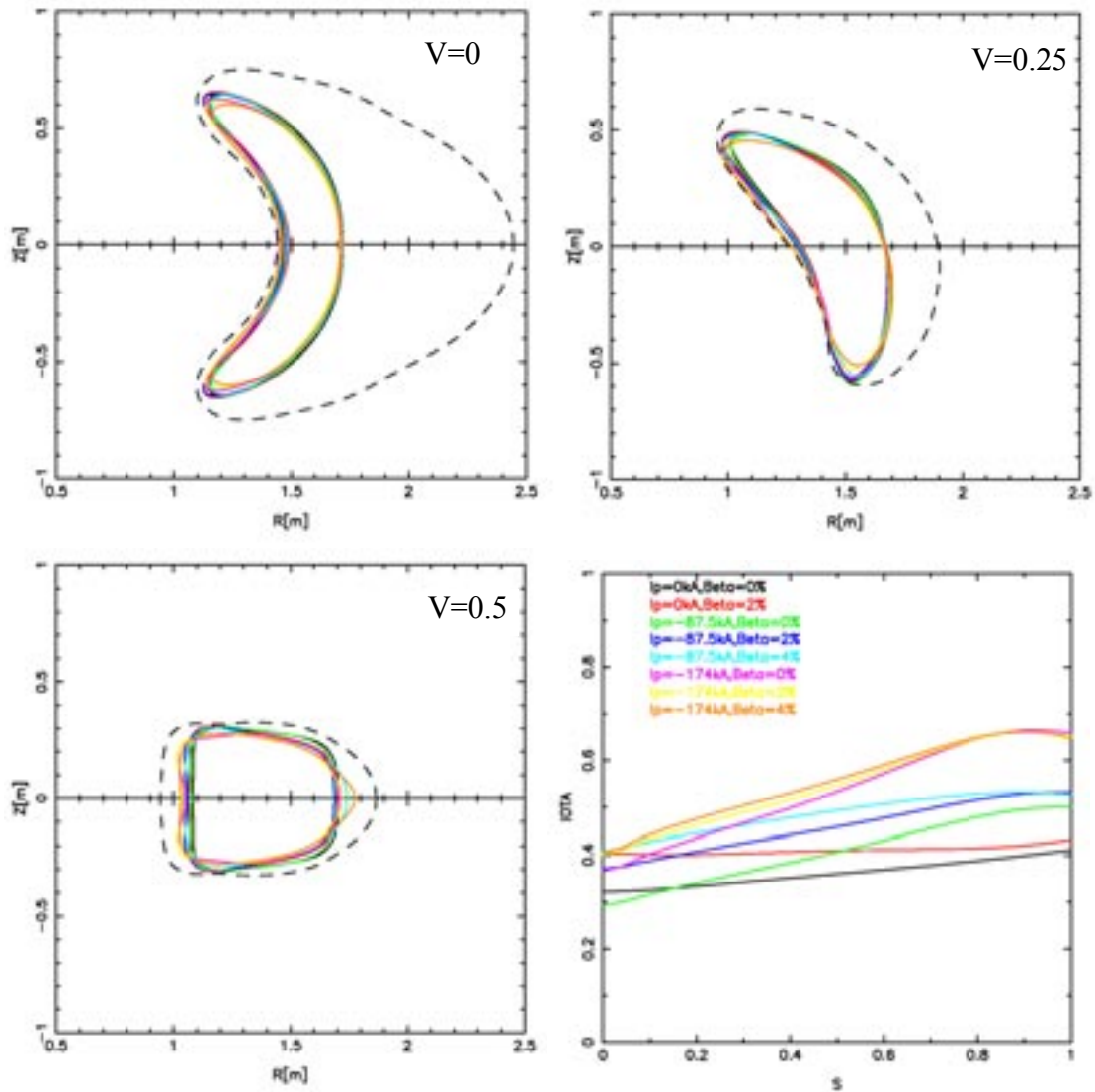
Figure 8-6. Overlay of plasma boundaries, and calculated iota profiles for various optimized equilibria from the I_p - β scan (Table 8-5). Note the wide range of iota profiles (shear and edge iota values) for which plasmas were found to be stable

8.4   Robustness of Performance as Plasma Profiles are Varied

For the results presented so far, the current and pressure profiles have had the same form as the reference li383 profiles. Now we investigate the effect on plasma performance of choosing plasma profiles that are different from the reference profiles. First, we examine the performance of plasmas supported by NCSX coils for a range of current profiles, fixing the pressure profile equal to the reference form shown in Figure 8-3. The effect of varying the current profile in the core region of the plasma is considered separately from the effect of varying the current profile in the edge region. In another set of experiments the effect of varying the pressure profile is considered, with the current profile held fixed equal to its reference form, also shown in Figure 8-3. We will show that good plasma performance is obtained for a wide range of current and pressure profiles. The results allay concern that the optimization methods used for designing the plasma configuration and coil system may have produced only a narrow operating space of good performance plasmas.

8.4.1   Variation of the Current Profile in the Core Region

Here we examine the performance of plasmas supported by NCSX coils for current profiles which differ from the reference form mainly in the core region. A 1-parameter family of current profiles, J_α, is conveniently defined by

$$J_\alpha (s) = (1-\alpha)\, J^{ref}(s) + \alpha\, J^{peaked}(s), \tag{8.4-1}$$

where $0 \leq \alpha \leq 1$, and J(s) denotes the surface averaged parallel current profile $\mathbf{J}\langle\ \mathbf{B}$. As α ranges from zero to one, J_α undergoes a substantial change in shape, from the reference hollow current profile, J^{ref} of Figure 8-3, to a peaked current profile defined as $J^{ref} = 1 - s^2$. A plot of the J_α for different α is shown in Figure 8-7.

With $\alpha = 0.0$, $J_\alpha = J^{ref}$ and the plasma configuration is identical to the reference configuration. As discussed in Section 8.3, the free-boundary β-limit for these profiles is at least $\beta = 5.0\%$. For $\alpha > 0$ we execute a sequence of free-boundary optimizer runs, increasing α from 0.0 in steps of 0.1, to determine the range of values of α (i.e., range of current profiles) for which NCSX plasmas are stable at $\beta = 3.0\%$. For each run, the plasma current was held fixed at $I_p =$ -174 kA, and the average toroidal field at R = 1.4 m is $B_T = 1.7$ T.
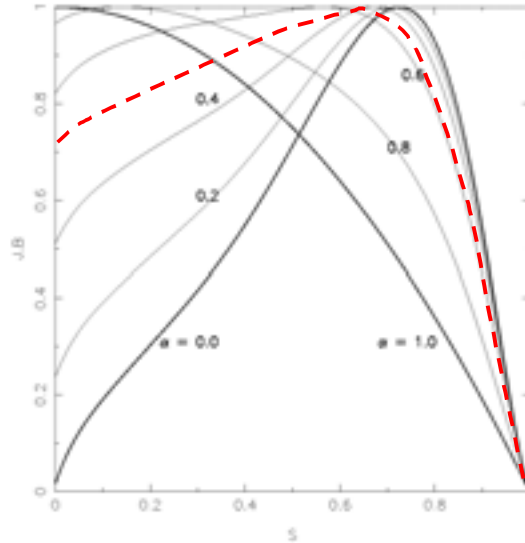
Figure 8-7. A 1-parameter family of current profiles which differ mainly in the core region . The stable range of current profiles is $0 \leq \alpha \leq 0.5$. The $\alpha = 0.5$ profile is shown as a dashed red curve. For the stable range of α, the internal inductance l_i of an equivalent tokamak with the same average elongation, triangularity, and aspect ratio ranges from 0.30 to 0.54

Table 8-7 shows a summary of the kink and ballooning stability properties for the various optimized configurations, including values of the effective ripple ε_h. It is seen that current profiles with $0 \leq \alpha \leq 0.5$ are stable to kink and ballooning modes, with quasi-axisymmetry measure $\varepsilon_h < 0.5\%$ at s=0.5. This wide range of stable profiles at $\beta = 3\%$ is the same as that presented at the PVR.

$\alpha= 0.0$	0.1	0.2	0.3	0.4	0.5	0.6
Kink: S	Kink: S	Kink: S	Kink: S	Kink: S	Kink: S	Kink:
Balloon: S	Balloon: S	Balloon: S	Balloon: S	Balloon: S	Balloon: S	
ε_h [%] = 0.19	ε_h [%] = 0.18	ε_h [%] = 0.18	ε_h [%] = 0.19	ε_h [%] = 0.20	ε_h [%] = 0.21	U
0.40	0.40	0.42	0.45	0.49	0.49	
1.04	1.12	1.25	1.36	1.42	1.38	

Table 8-7. Stability properties and effective helical ripple, ε_h[%], at s=0.3, s=0.5, and s=0.8 for current profiles parameterized by peakedness parameter α (see Eq. 8-4.1 and Figure 8-7). All equilibria correspond to $I_p = -174$ kA, $\beta = 3.0\%$, with $B_T = 1.7$ T at R = 1.4 m. The stable range of α is $0 \leq \alpha \leq 0.5$

Table 8-8 shows a summary of the coil current changes required to maintain stable equilibria while accommodating the profile changes. The current changes are small, with the maximum change in coil current occuring, as expected, for the limiting case α=0.5 where the optimizer has the most difficulty in stabilizing the plasma.

ΔI_{M1} [kA-turns]	ΔI_{M2} [kA-turns]	ΔI_{M3} [kA-turns]	ΔI_{TF} [kA-turns]	ΔI_{PF3} [kA-turns]	ΔI_{PF4} [kA-turns]	ΔI_{PF5} [kA-turns]	ΔI_{PF6} [kA-turns]
+26.	+5.	+3.	+4.	+0.	+0.	+8.	+1.
-4.	-4.	-1.	-1.	-8.	-168.	-0.	-0.

Table 8-8. Coil current variation for the current profile scans. In each column is shown the max +/- variation in the current for coil "k" compared with the current required to support the α=0 state.

Figure 8-8 shows an overlay of plasma boundaries and calculated iota profiles for the α sequence of stable configurations. The variation in plasma boundary shape is seen to be very small; however the variation in the shear of the iota profile is substantial. As α increases and current is added to the core region of the plasma, the axis value of iota increases. The edge iota, although unconstrained in the present optimization runs, remains nearly constant. The onset of instability as α is raised to α = 0.5 may be correlated with a lack of adequate shear in the iota profile. On the other hand, we see from the $\iota(s)$ plots of the I_p = -174kA, β=0%, 2% and 4% sequence of marginally stable equilibria shown in Figure 8-6 that such an assumption may be presumptive. Further study is needed to confirm such a conclusion.
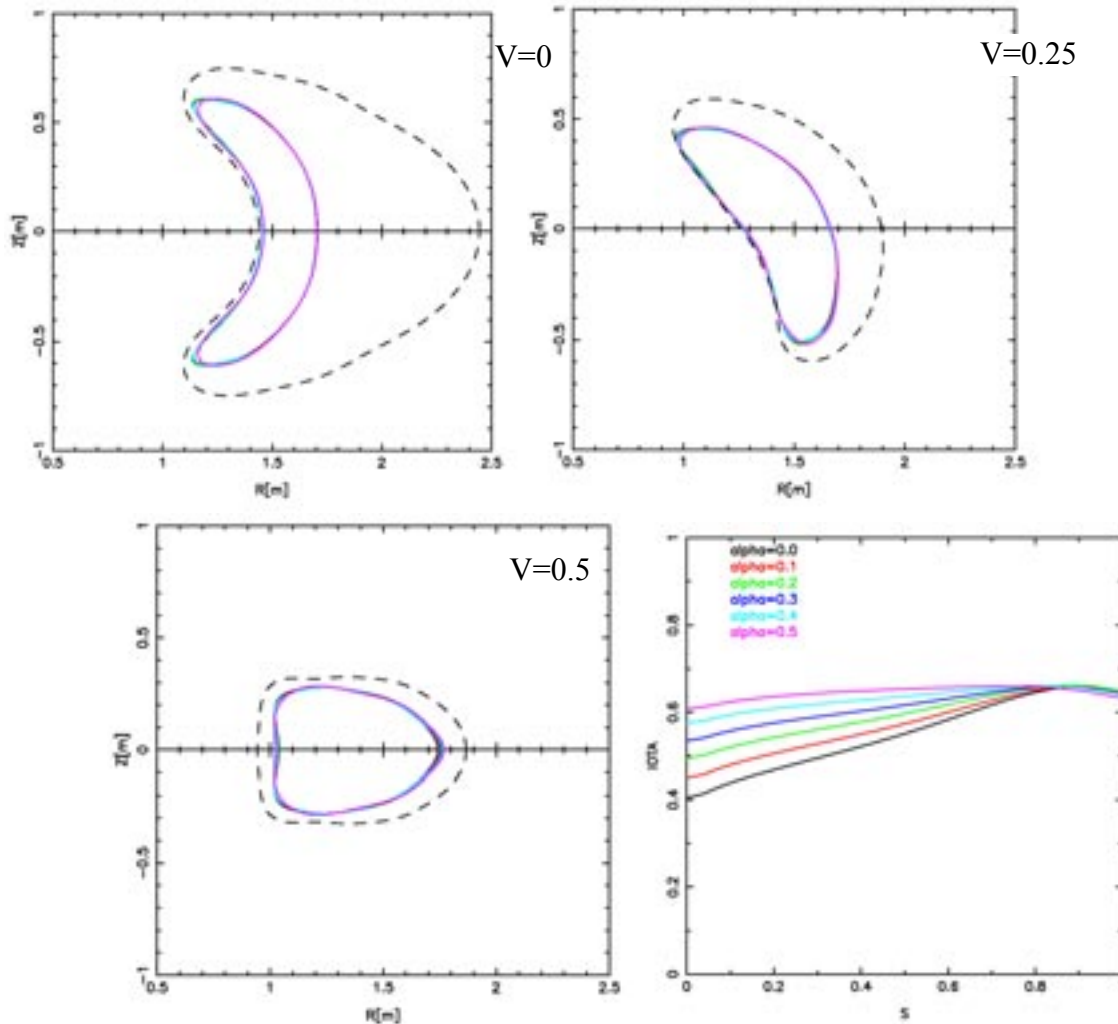
Figure 8-8. Overlay of plasma boundaries for stable equilibria at β = 3.0% for the J_α sequence of current profiles (where $J\langle B$ is varied in the core region). The calculated iota profiles are also shown.

8.4.2 Variation of the Current Profile in the Edge Region

We now explore the effect of varying the current profile in the edge region. In particular we consider the family of current profiles, J_δ, shown in Figure 8-9 where

$$J_\delta (s) \propto J^{ref}(s) + \delta\, J^{edge}(s), \tag{8.4-2}$$

and $J^{edge}(s) = s^{10}$. Such a parameterization allows a sizeable current density near the plasma edge. The values of δ shown in Figure 8-9 represent the magnitude of J_δ at the plasma edge relative to the maximum value of J_δ (s). δ varies from 0.0 to 0.5 in steps of 0.1.
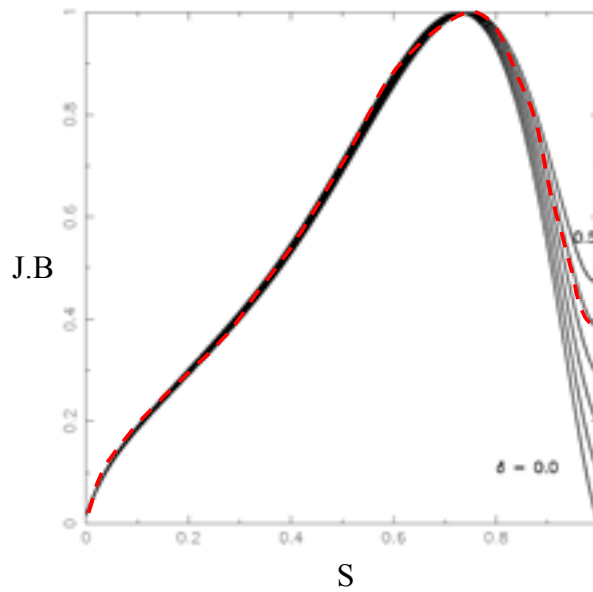
Figure 8-9. Family of current profiles J$_\delta$ (s) which vary mainly in the edge region. Stability may be enhanced as the edge current builds due to an increase in the global shear.

Whereas in Section 8.4.1 we considered free-boundary equilibrium reconstructions at β = 3.0%, in this Section we examine the stability characteristics of finite edge current free-boundary plasmas at β = 5.0%, a value which exceeds the reference fixed-boundary β-limit for li383.

Already the I$_p$ - β scan presented in Table 8-5 has shown a stable configuration with I$_p$ = -174 kA, β = 5.0%. The coil currents for this δ = 0.0 configuration are shown in Table 8-9. Using the same coil currents, free-boundary equilibria were calculated for each of the current profiles shown in Figure 8-9. In each case I$_p$ = 174 kA, β = 5.0%, with B$_T$ = 1.7 T at R = 1.4 m, and the pressure profile was fixed equal to the reference form. Remarkably, each current profile for the new calculated equilibrium is found to be stable to kink and ballooning modes.

M 1 [kA-turns]	M 2 [kA-turns]	M 3 [kA-turns]	TF [kA-turns]	PF3 [kA-turns]	PF4 [kA-turns]	PF5 [kA-turns]	PF6 [kA-turns]
655.8	651.2	524.3	58.6	1230.3	447.9	79.9	-1.3

Table 8-9. Coil currents corresponding to the stable configuration with I$_p$ = -174 kA, β = 5.0% presented in Table 8-5.   These currents are used in free-boundary equilibrium reconstructions which vary the edge current density.

The robust stability for the sequence of equilibria with different edge current densities can perhaps be understood in terms of the effect on the iota profile of adding successive current layers to the plasma edge region. Figure 8-10 shows overlays of the plasma boundaries and profiles of $\iota(s)$ for the equilibria with $\delta = 0.0$, 0.2, and 0.4. It should be noted that as more edge current is included, the shear $d\iota/ds$ in the edge region of the plasma is increased with no change in the edge iota. Such an increase in shear is known to be stabilizing for current-carrying stellarators (see Ref. [2] and results presented in Chapter 4).

An increase in current density near the plasma edge is an expected consequence of a transition from L-Mode to H-Mode profiles. In view of the observations made above, there is an interesting possibility that such a transition will have beneficial effects on MHD stability. Future calculations should calculate β-limits for realistic models of H-mode profiles in NCSX.

In Figure 8-10 we present, for comparison, the plasma boundary and iota profile for the reference S3 equilibrium corresponding to $\beta=4\%$, $\delta=0.0$. It is interesting to observe that the edge iota values for the $\beta = 4\%$ and $\beta=5\%$ equilibria are quite different; $\iota_{max} \approx 2/3 = .67$ for the S3 equilibrium with $\beta = 4\%$, whereas $\iota_{max} \approx 3/5 = 0.60$ for the $\beta = 5\%$ equilibria. It appears that the preferred shape for the $\beta = 5\%$ configuration is one that avoids having $\iota = 3/5$ in the plasma region; STELLOPT adjusts the coil currents in such a way as to accommodate this preference. Similar observations have been made for configurations obtained in the $I_p - \beta$ scan; for fixed β of 4.0%, if I_p is raised in small increments from -131 kA to –174 kA, configurations optimized for stability and quasi-axisymmetry have ι_{max} values that change abruptly from 0.60 to 0.67. No intermediate values of ι_{max} are found. This appears to be due to the **simultaneous** optimization of stability **and** QA-ness; If the weighting of the QA contribution to the STELLOPT cost function is decreased while preserving the same weighting for the stability cost function, configurations with any chosen value of ι_{max} between 0.60 and 0.67 are obtained using the edge-ι control procedure discussed in Section 8.5.
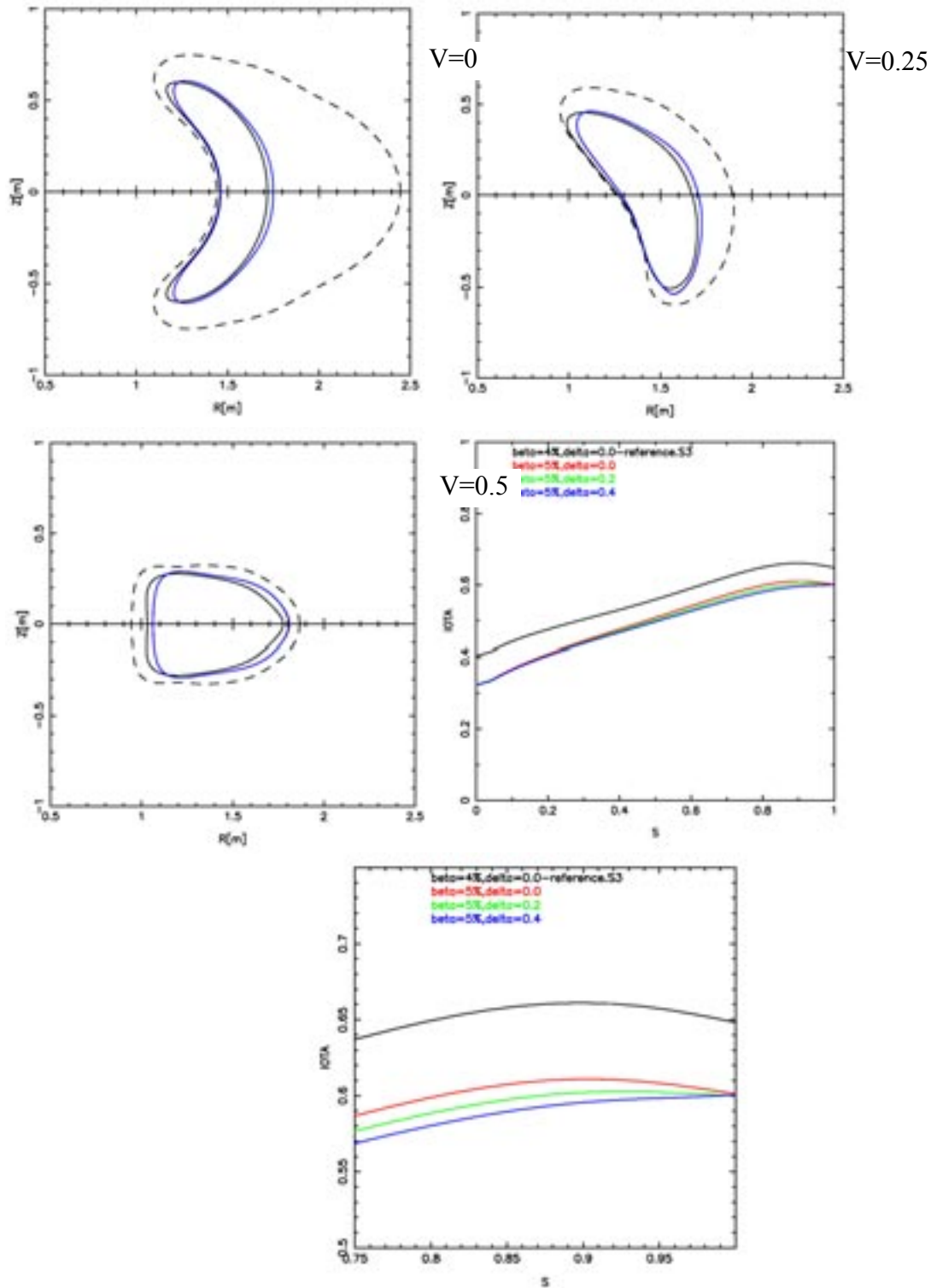
Figure 8-10. Overlay of three plasma boundaries for stable equilibria at β = 5% with varying edge current densities (δ = 0.0, 0.2, 0.4). The coil currents are the same in all cases. The plasma boundaries vary little. Also shown are the ι(s) profiles (shown plotted in two frames, the second of which is a blow-up of the first) from which the increase in edge shear is evident. Also shown is the plasma boundary and iota profiles for the reference S3 state with β = 4%.

8.4.3 Variation of the Pressure Profile

As another set of numerical experiments we examine the performance of plasmas supported by NCSX coils for a range of pressure profiles. The current profile shape is held fixed equal to the reference form. First, a 1-parameter family of pressure profiles is defined by

$$p_\gamma(s) = (1 - \gamma) \, p^{ref}(s) + \gamma \, p^{peaked}(s), \qquad\qquad (8.4\text{-}3)$$

where $0 < \gamma < 1$. As γ ranges from zero to one, p_γ undergoes a change from the (broad) reference pressure profile to a more peaked pressure profile whose analytic dependence on toroidal flux is chosen to be $p^{peaked} \propto (1 - s)^2$. This "peaked" form is a good fit with the NBI heated PBX-M discharge profile denoted by p_B in Section 8.2. A plot of the p_γ for different values of γ is shown as the black curves in Figure 8-11. The p_γ profiles all have zero pressure gradient at the plasma edge, $s=1$.

A sequence of free-boundary optimizer runs was executed at $\beta = 3.0\%$ increasing γ from 0.0 to 1.0 in steps of 0.2 to determine the range of pressure profiles for which NCSX plasmas supported by the designed coils are stable to ballooning and kink modes with optimized QA. As in Section 8.4.1, we choose $I_p = -174$ kA, $\beta = 3.0\%$ with $B_T = 1.7$ T at $R = 1.4$ m, making no attempt to optimize β by changing I_p from this reference value.

Table 8-10 summarizes the optimizer runs as the peakedness parameter γ is varied. For the given parameterization of p(s), stable configurations with good quasi-axisymmetry ($\varepsilon_h < 0.5\%$ at s=0.5) were found for all cases except $\gamma =1.0$. For this case, we have found a stable configuration at $\beta = 2.5\%$. Figure 8-12 shows an overlay of the plasmas boundaries and iota profiles for each of the stable optimized configurations with $\gamma \leq 0.8$. One sees little change in the optimized plasma shape for these changes in pressure profile. Table 8-11 shows a summary of the coil current changes required to maintain the stable equilibria for the various pressure profiles. Consistent with the small plasma shape changes, the current changes are also small.

The effect on performance of including a finite edge pressure gradient was also investigated using a profile form defined by

$$p_{pedestal}(s) = p^{ref}(s) + c \, s^7(1\text{-}s^3) \, , \qquad\qquad (8.4\text{-}4)$$

with coefficient c adjusted to give a desired edge pressure gradient.

A sequence of optimizer runs was executed using pressure profiles of the form Eq. 8.4-4. A configuration, stable at $\beta = 3\%$ and with good QA measure $\varepsilon_{eff} = 0.56\%$, was obtained for the pedestal profile shown in red in Figure 8-11. For this profile, the chosen c gives $(dp/ds)/p_0|_{s=1} = -2.2$. The coil currents for this configuration were included in the data for Table 8-11,
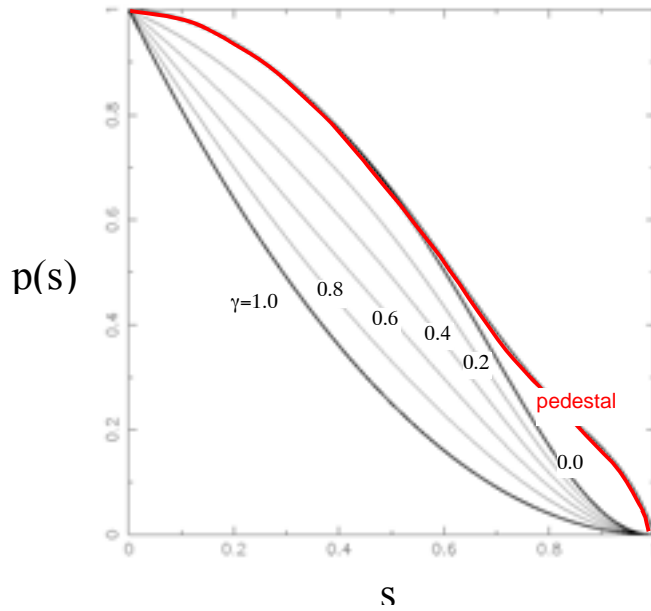
Figure 8-11. The 1-parameter family of pressure profiles, P_γ, for which plasma performance is evaluated at $\beta = 3\%$. $\gamma = 0.0$ is the reference profile. In red is shown the edge pedestal profile for which a stable configuration was also obtained at $\beta = 3\%$.

$\gamma= 0.0$	0.2	0.4	0.6	0.8	1.0
Kink: S Balloon: S ε_h [%] = 0.19 0.40 1.04	Kink: S Balloon: S ε_h [%] =0.19 0.40 1.01	Kink: S Balloon: S ε_h [%] =0.21 0.43 1.04	Kink: S Balloon: S ε_h [%] =0.23 0.43 1.06	Kink: S Balloon: S ε_h [%] = 0.23 0.40 0.92	Kink: U Balloon:U on surfaces 2,3 only

Table 8-10. Stability properties and effective helical ripple, ε_h[%], at s=0.3, s=0.5, and s=0.8 for pressure profiles parameterized by peakedness parameter δ (see Eq. 8.4-1 and Figure 8-11). All equilibria correspond to $I_p = $-174 kA, $\beta = 3.0\%$, with $B_T = 1.7$ T at R = 1.4 m. The stable range of δ is $0 \leq \delta \leq 0.8$ All equilibria correspond to $\beta = 3.0\%$.

The operating space of stable configurations with $\beta = 3.0\%$, including substantial variations in current and pressure profiles, and good quasi-symmetry, appears to be broad. We also note that it should be possible to widen the operating space of stable profiles defined above by allowing the plasma current to vary in addition to the shape.

ΔI_{M1} [kA-turns]	ΔI_{M2} [kA-turns]	ΔI_{M3} [kA-turns]	ΔI_{TF} [kA-turns]	ΔI_{PF3} [kA-turns]	ΔI_{PF4} [kA-turns]	ΔI_{PF5} [kA-turns]	ΔI_{PF6} [kA-turns]
+17.	+19.	+12.	+3.	+0.	+4.	+6.	+3.
-3.	-3.	-14.	-9.	-0.	-308.	-32.	-0.

Table 8-11. Coil current variation for the pressure profile scans. In each column is shown the max +/- variation in the current for coil "k" compared with the current required to support the δ=0 state.
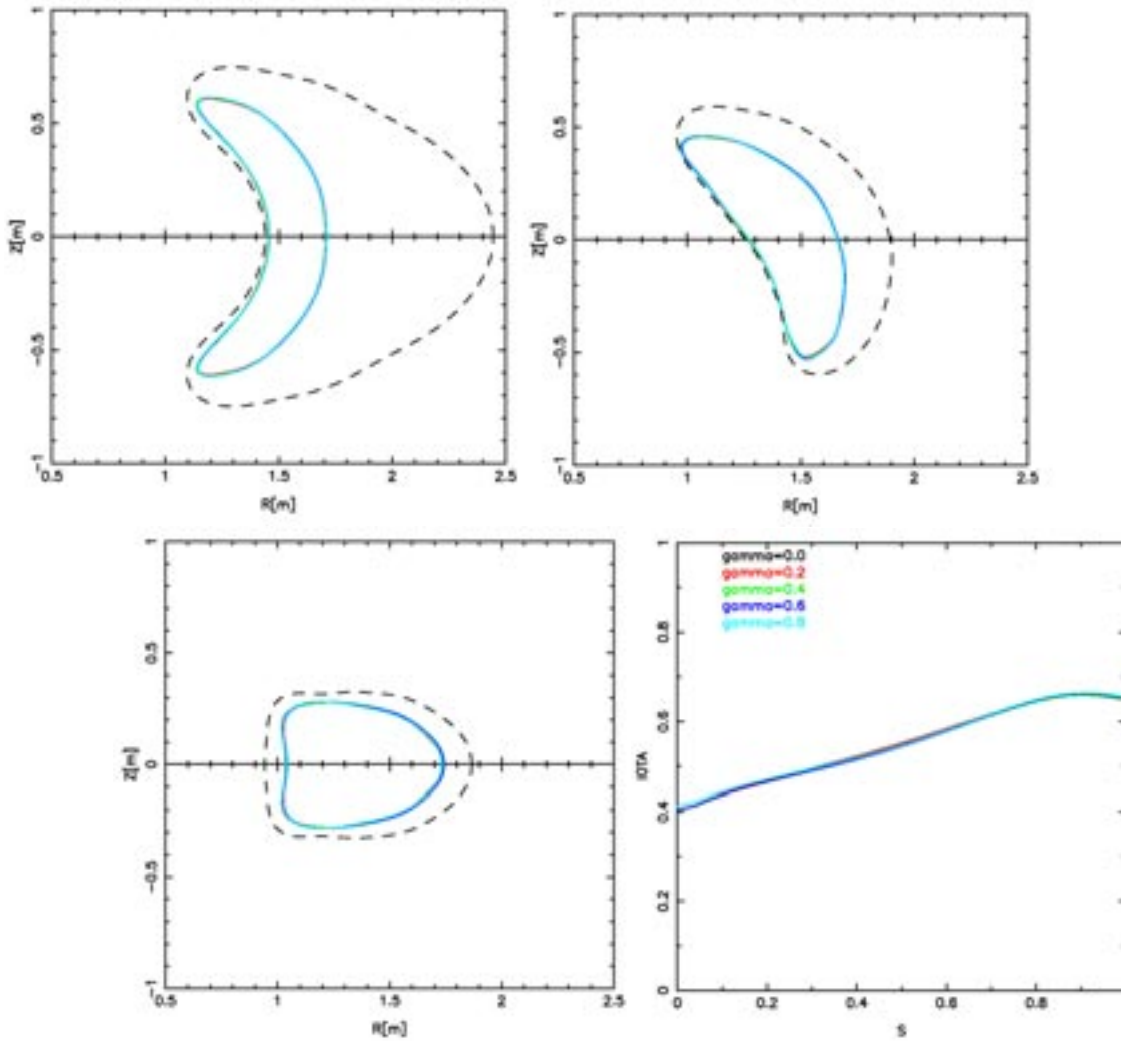
Figure 8-12. Overlay of plasma boundaries and iota profiles for stable optimized configurations of the pressure profile scan. I_p = -174 kA, β = 3.0% for all cases.

8.5   Flexibility to Control the External Transform

We now demonstrate the capability of NCSX coils to effect substantial changes in the external field contribution to $\iota(s)$. The MHD stability of stellarator plasmas can depend critically on details of the iota profile; for example on the location of the $\iota= 0.5$ magnetic surface. The W7AS experiments reported at IAEA2000 in Sorrento [3] demonstrate cases where stability depends, not on the magnitude of the external transform ι_{ext}, but on the ability to avoid $\iota = 0.5$ in the plasma and hence q=2 global tearing modes. The reference S3 configuration for NCSX has $\iota(0) = 0.40$, $\iota(1) = 0.65$. A natural S1 "vacuum" configuration asssociated with S3, obtained by running STELLOPT with $I_p = 0$ kA, $\beta = 0\%$ and optimizing coil currents for QA transport with no constraints on iota yields the configuration tabulated in Table 8-5 with $\iota(0) = 0.34$, $\iota(1)$ = 0.42 => $\iota(s)$ < 0.5 for all s values. Plasma evolution from this S1 state to the reference S3 implies passage through $\iota(1) = 0.5$. The results of Section 8-3 suggest that NCSX coil currents can be chosen to evolve in such a way that 3D shaping of the plasma avoids the trigger of any kink mode (for example evolution through states corresponding to the "diagonal" sequence in Table 8-5 where $\beta \propto I_p$). Nevertheless it is important to have the ability to control the iota profile through external shaping so that $\iota(1) = 0.5$ can be avoided, if that is found to be necessary in the actual experiment. This capability is exploited in Chapter 9.4 where a "high iota" startup scenario is presented which avoids passage through $\iota(1) = 0.5$. The ability to control $\iota(s)$ is also a very useful control knob to aid the mapping of stable/unstable boundaries for NCSX.

8.5.1   Variation of $\iota(s)$ at Fixed Shear

Here we demonstrate the ability to raise and lower $\iota(s)$ while keeping the shear essentially constant. As a baseline plasma whose iota profile is to be changed we choose the reference S3 state with $I_p = -174$ kA, $\beta = 4.2\%$, and axis/edge iota values of $\iota(0) = 0.40/\iota(1) = 0.65$, respectively. The choice of baseline plasma for the iota flexibility experiments is arbitrary, since in an actual experiment we may be interested in exploring the effects of changing the iota profile for a variety of plasma states. For the iota scan experiments we target desired changes in $\iota(0)$ and $\iota(1)$ relative to the baseline values, and optimize χ^2_{Bmn} making no attempt to stabilize the kink and ballooning modes; the goal here is to explore coil flexibility, not plasma performance. The plasma current is held fixed at $I_p = -174$ kA, and the toroidally averaged B_T is held constant at 1.7 T at R = 1.4 m. We seek to change $\iota(s)$ at fixed plasma current and toroidal field by 3D shaping only. All configurations are further constrained by the first wall PFC boundary.

Figure 8-13 shows plasma boundaries and calculated iota profiles for cases where $\iota(0)$ and $\iota(1)$ were programmed to change by equal amounts so as to keep the shear constant. Substantial changes $\Delta\iota(s) \in [-0.2, +0.1]$ relative to the baseline are shown possible. The required coil currents to effect these changes are shown in Table 8-10. We note the range of shapes required to produce the target iota profiles and the correlation of shape with the limits on the range of $\Delta\iota(s)$. For $\Delta\iota(s) = +0.1$ (red curves in Figure 8-13) the plasma cross section at the v=1 symmetry plane has an extremely pointed nose region. Not only does this present numerical difficulties for the VMEC equilibrium solver, but one must eventually worry about the viability of such a shape on physics grounds, for example on account of neutral penetration. For $\Delta\iota(s) = -0.2$ (blue curves) the same cross section shows a square shape so now the plasma is confronted

with the problem of how to fit within the given bullet shape of the first wall PFC boundary at v=0.5 – a square peg in a round hole problem! For the above reasons, one must expect that the range of achievable $\Delta\iota$(s) depends on the details of the baseline plasma.
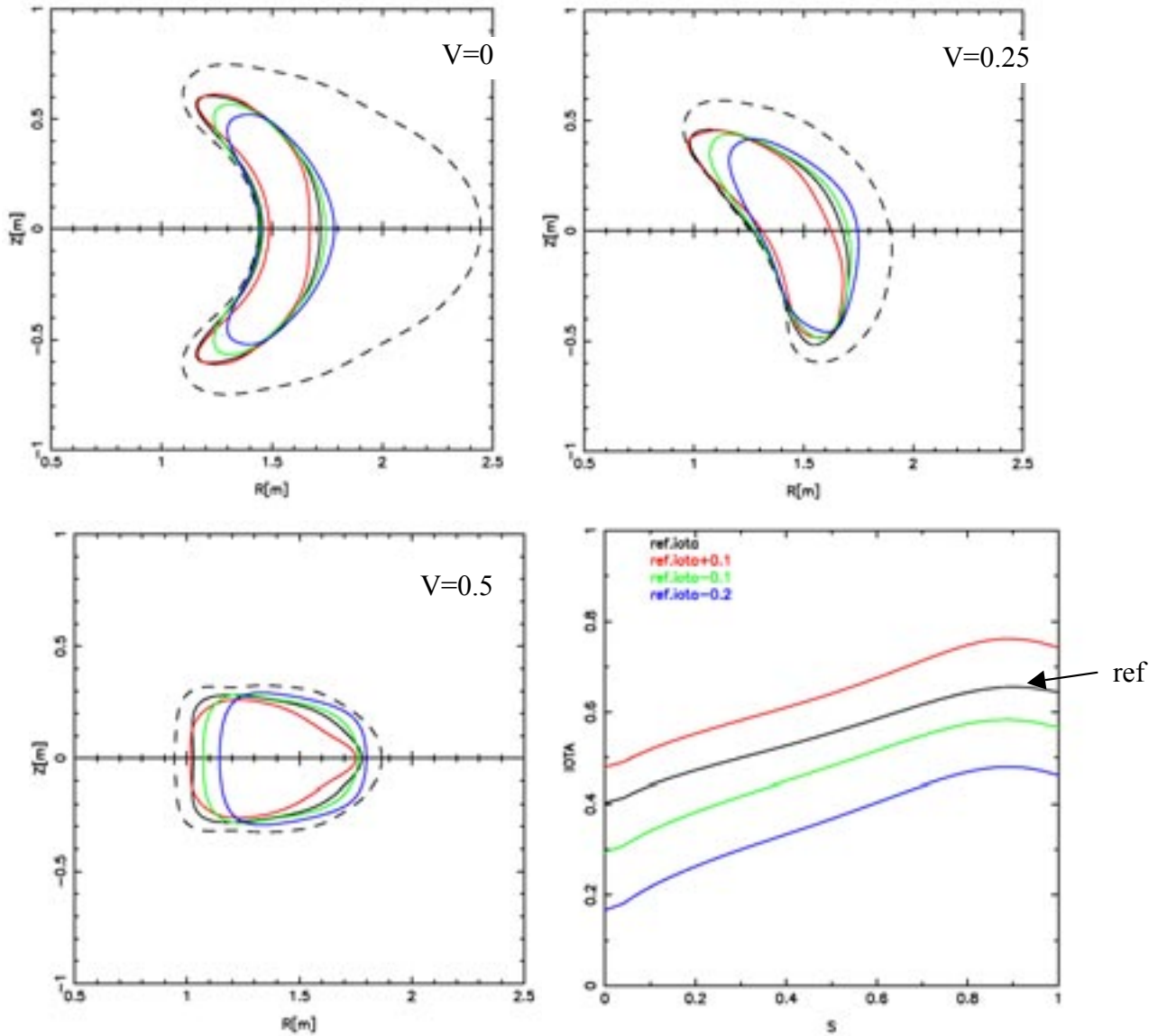
Figure 8-13. Plasma boundaries and iota profiles for iota-scan flexibility studies where coil currents are asked to change in such a way as to induce specified changes in ι(s). Here ι(s) is raised/lowered in such a way that the shear is preserved

$\Delta\iota(s)$	ΔI_{M1} [kA-turns]	ΔI_{M2} [kA-turns]	ΔI_{M3} [kA-turns]	ΔI_{TF} [kA-turns]	ΔI_{PF3} [kA-turns]	ΔI_{PF4} [kA-turns]	ΔI_{PF5} [kA-turns]	ΔI_{PF6} [kA-turns]
+0.1	+65.	+60.	+75.	-67.	0.	-1021.	+113.	+1.
-0.1	-78.	-61.	-66.	+73.	0.	-393.	-33.	+0.
-0.2	-181.	-157.	-161.	+167.	-1684.	-947.	-40.	+7.

Table 8-10. Coil current variation for raising/lowering $\iota(s)$ at constant shear (see Figure 8-13)
Current differences are from the reference S3 state

8.5.2 Variation of $\iota(s)$ at Fixed $\iota(0)$ – Changing the Shear

Figure 8-14 and Table 8-11 show results from a similar calculation, where coil currents are adjusted so that the axis value $\iota(0)$ remains fixed at the nominal value $\iota(0) = 0.40$ and the edge iota is increased/decreased from the nominal value of $\iota(1) = 0.65$, thereby inducing a change in shear. The plasma current, toroidal field, plasma profiles and β are held fixed so that the plasma contribution to iota, $\iota_p(s)$, remains essentially constant. Any change in $\iota(s)$ is due to the induced change in the external transform, $\iota_{ext}(s)$.

$\Delta\iota(1)$	ΔI_{M1} [kA-turns]	ΔI_{M2} [kA-turns]	ΔI_{M3} [kA-turns]	ΔI_{TF} [kA-turns]	ΔI_{PF3} [kA-turns]	ΔI_{PF4} [kA-turns]	ΔI_{PF5} [kA-turns]	ΔI_{PF6} [kA-turns]
-0.07	-218.	+309.	-139.	+15.	0.	-1161.	+68.	+0.
+0.1	+40.	+20.	-13.	-19.	0.	-617.	-35.	+0.
+0.2	+64.	+1.	+17.	-29.	0.	-1219.	-94.	-2.

Table 8-11. Coil currents for decreasing/increasing shear (see Figure 8-14)

The range of shear accommodated by the coils is $\int = (\iota_{max} - \iota(0))/s_m = 0.23 \rightarrow 0.53$, where s_m is the value of scaled toroidal flux, s, where ι is maximum. The ability to reduce the

shear relative to the chosen baseline plasma is seen to be quite modest. The main impediment to shear reduction is the first wall boundary location. Configurations with lower shear have been produced by the M45 coils but they tend to overlap the first wall boundary near the top/bottom of the inboard major radius (eg see limiting plasmas at v=0 and v=0.5 symmetry cross sections in Figure 8-14).

The results in this Section demonstrate a substantial capability for the M45 coil set to change the iota profile for fixed I_p, B_T, plasma profiles and β. We have found similar flexibility to change the $\iota(s)$ profile for S1 states with $I_p = 0$ kA, a flexibility that is used to control $\iota(s)$ in the high-iota startup scenario presented in Chapter 9.
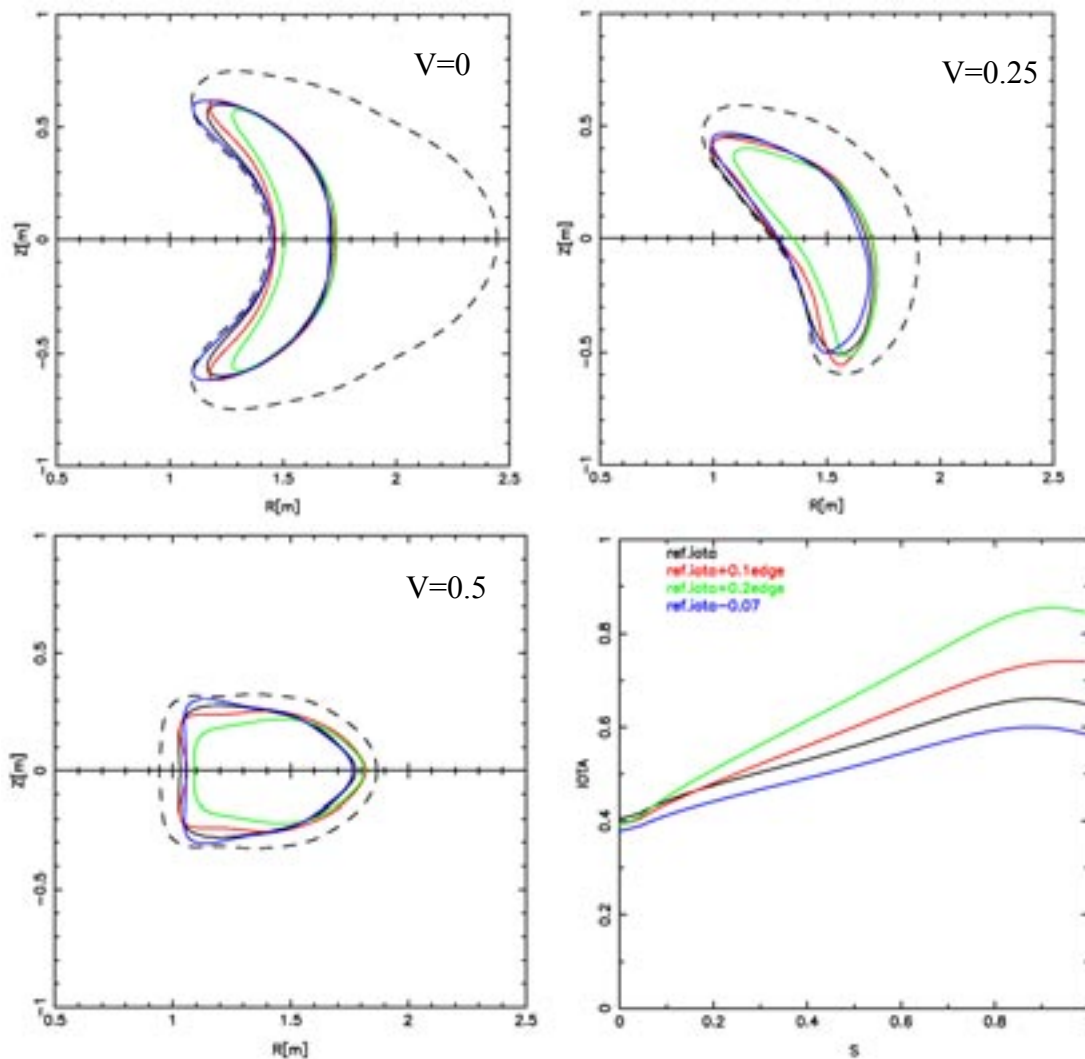
Figure 8-14. Plasma boundaries and iota profiles for iota-scan flexibility studies where coil currents are asked to change in such a way as to induce specified changes in ι(s). Here the shear is increased/decreased

8.6 Flexibility to Study Kink Stabilization by 3D Shaping

The free-boundary I_p - β scan numerical experiments presented in the Section 8.3 and summarized in Table 8-5 can be used to demonstrate the effect of MHD stabilization by 3D shaping and to suggest controlled experiments to explore stability boundaries in NCSX exploting the flexibility of the coil system.

Consider two configurations obtained by STELLOPT using the heavyside cost function measure of stability that have the same value of plasma current but different values of beta. For example configurations with I_p = -44.0 kA, β = 1.0%, and I_p = -44.0 kA, β = 3.0%. As discussed in Section 8.2, any stable "final state" of the optimizer using the heavyside feature is a state of marginal stability. Each plasma is at the β-limit for its given shape and profiles; the plasma profiles are the same yet the plasma shapes are quite different (see Figure 8-15). Axis and edge iota values are:

$\iota(0) = 0.42$, $\iota(1) = 0.52$ for I_p = -44.0 kA, β = 1.0%,
$\iota(0) = 0.41$, $\iota(1) = 0.46$ for I_p = -44.0 kA, β = 3.0%.

Now consider the effect of taking the I_p = -44.0 kA, β = 1.0% configuration and raising β to 3.0% while keeping the plasma boundary fixed. The iota profile for this β = 3.0% "virtual" configuration is found to have $\iota(0) = 0.42$, $\iota(1) = 0.51$, little changed from the free-boundary 1.0% configuration. However, the n=1 family of external kink modes is now strongly unstable as a result of the increase in β, with maximum eigenvalue λ^K_1 = -6.01e-4. Ballooning modes are also found over the split range of magnetic surfaces from s = 0.31 to s = 0.50 and from s = 0.86 to s = 0.96. It follows that the change in shape and the change in external transform associated with the change in coil current between the I_p = -44.0kA, β = 1.0% free-boundary configuration and the I_p = -44.0 kA, β = 3.0% free-boundary configuration are responsible for the stabilization of the higher β configuration; without this change of shape we would have obtained the unstable "virtual" configuration.

We have remarked that the $\iota(s)$ profile for the I_p = -44.0kA, β = 1.0% free-boundary configuration has $\iota(1) = 0.52$. The question naturally arises whether the reduced β-limit of this configuration compared with the I_p = -44.0 kA, β = 3.0% free-boundary configuration, which had $\iota(1) = 0.46$, is due to the destabilizing influence of the $\iota(1) = 1/2$ rational surface. The flexibility of the NCSX modular coil set to change the iota profile (demonstrated in Section 8.5) can be used to test such a question. The free-boundary optimizer was re-run for the case I_p = -44.0 kA, β = 1.0%, with the additional STELLOPT constraint that the coil currents produce a plasma shape with $\iota(1) = 0.46$ so that the ι = 0.5 surface is no longer in the plasma region. A successful solution was found with $\iota(0) = 0.35$, $\iota(1) = 0.47$. The coil currents for this modified configuration are shown in the third column of Table 8-12. Overlays of the modified I_p = -44.0 kA, β = 1.0% low β-limit configuration and the marginally stable I_p = -44.0 kA, β = 3.0% configuration, as well as the calculated $\iota(s)$ profiles are shown in Figure 8-16. Stabilization at the enhanced β is now clearly due to 3D shaping.

The ability to investigate the stabilizing role of 3D shaping is an important element of the experimental program of NCSX. Investigations of this type allow testing and investigation of the stability boundaries of NCSX at low β.

	M 1 [kA-turns]	M 2 [kA-turns]	M 3 [kA-turns]	TF [kA-turns]	PF3 [kA-turns]	PF4 [kA-turns]	PF5 [kA-turns]	PF6 [kA-turns]
I_P: -44.0 kA β: 1.0% ι(0): 0.42 ι(1): 0.52	827.1	776.8	380.0	-0.4	-1.4	+7.5	-0.0	+0.0
I_P: -44.0 kA β: 3.0% ι(0): 0.41 ι(1): 0.46	733.6	700.4	593.7	-13.0	-166.7	+134.7	+80.2	+0.4
I_P: -44.0 kA β: 1.0% ι(0): 0.35 ι(1): 0.47	659.9	670.0	655.7	-0.7	-1.4	+5.8	-0.1	+0.0

Table 8-12. Coil currents for cases illustrating MHD stabilization by 3D shaping. The color coding is consistent with Figures 8-15 and 8-16.
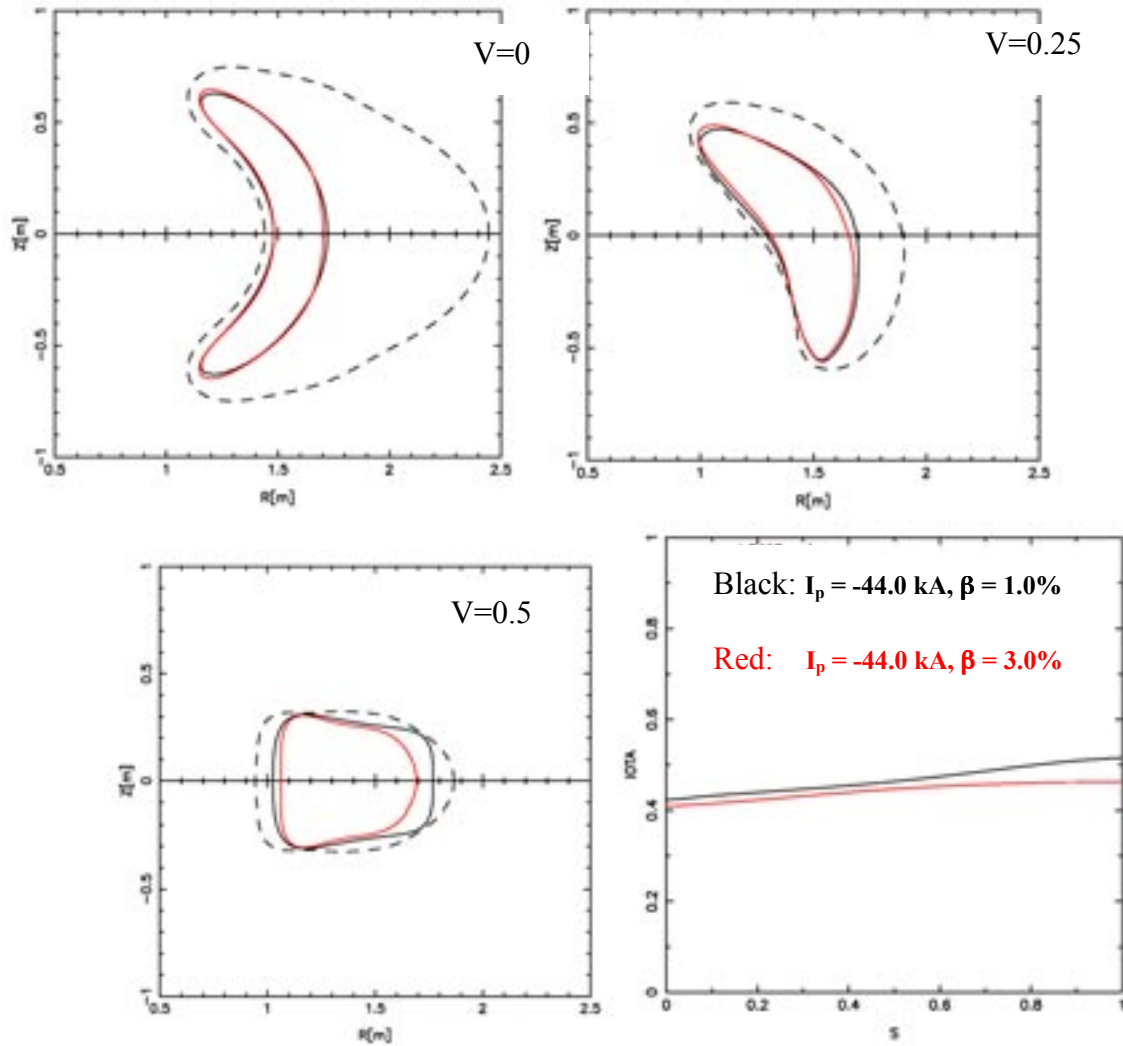
Figure 8-15. Overlay of plasma boundaries and iota profiles for the cases
$I_p = -44.0$ kA, $\beta = 1.0\%$ (black) and $I_p = -44.0$ kA, $\beta = 3.0\%$ (red) used to illustrate MHD stabilization by 3D shaping. Each configuration is at the β-limit for its given shape and profiles. Profiles are the same for the two configurations, suggesting that the possibility that the enhanced β-limit of the 3% configuration is due to the difference in shape. However the iota profiles are different for the two configurations and one needs to show that the difference in β–limit is not due to an artificially low limit for the 1% configuration because $\iota = 0.5$ is in the edge region of the plasma.
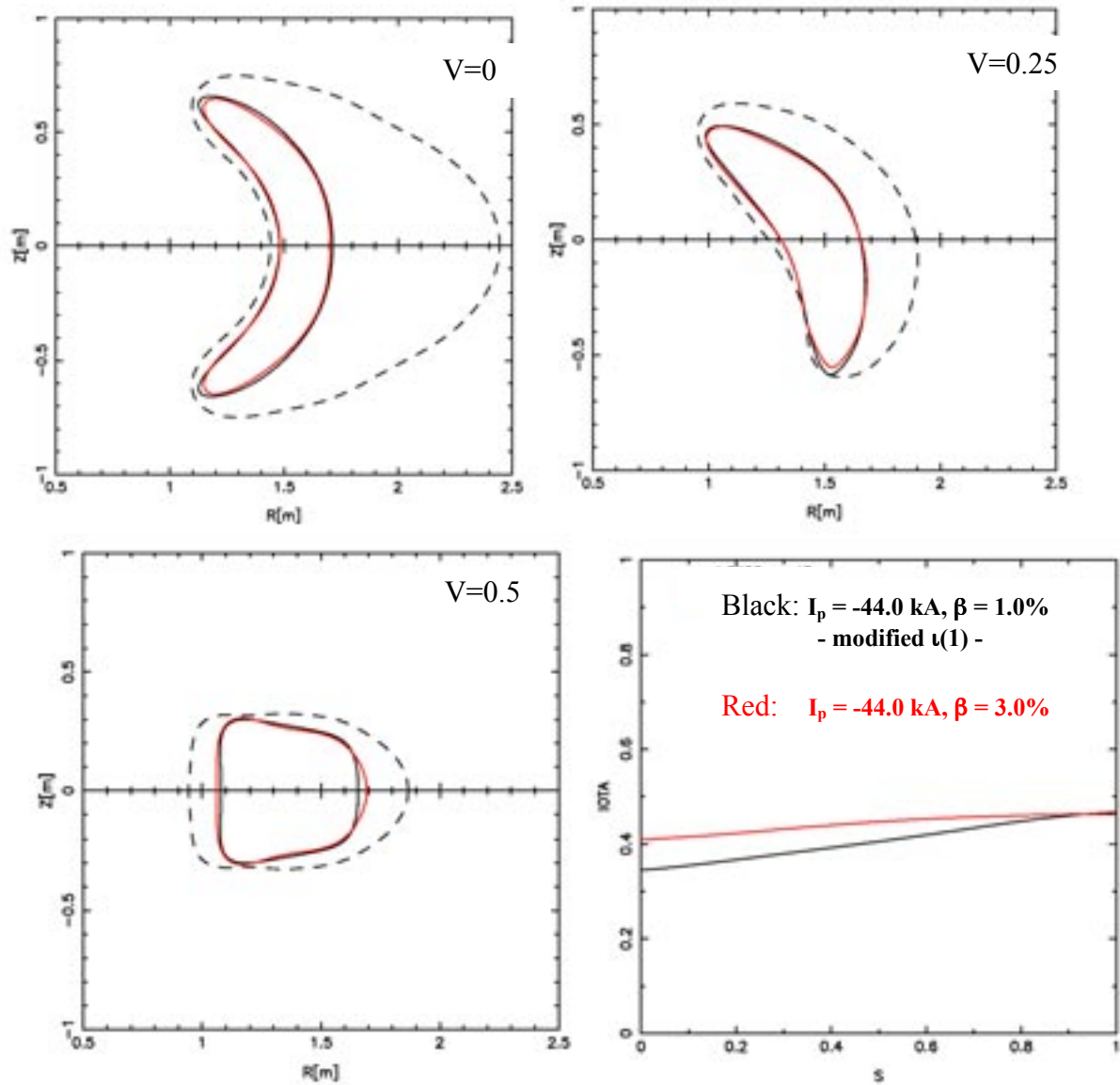
Figure 8-16. The iota profile of the $I_p = -44.0$ kA, $\beta = 1.0\%$ configuration is modified by 3D shaping so that the edge iota is lowered to equal that of the $I_p = -44.0$ kA, $\beta = 3.0\%$ configuration (see Figure 8-15). The $\iota = 0.5$ surface now lies outside the plasma, showing that the β-limit of the $\beta = 1\%$ configuration differs from that of the $\beta = 3\%$ configuration due to a difference in shape, not the proximity of $\iota(1)$ to 0.5.

8.7 Flexibility to Vary the Degree of Quasi-Axisymmetry

The ability to generate configurations with good quasi-axisymmetry is an essential requirement of the NCSX design. For a systematic exploration of the role of QA in improving the transport properties of stellarator plasmas, it is necessary to have the ability to control the degree of QA-ness. In this Section we demonstrate this ability, by varying NCSX modular coil currents to induce plasma shape changes that degrade/enhance the QA-ness (measured by the

magnitude of the ripple amplitude, ε_h) while maintaining plasma stability to kink and ballooning modes.

Figure 8-17 shows an overlay of plasma boundaries for three configurations, each with $I_p = -87.5$ kA, $\beta = 2.0\%$, each with the same profiles of plasma current and pressure, but each exhibiting different degrees of quasi-axisymmetry. The ripple amplitude ε_h varies by a factor of fourteen at the s=0.3 surface, by a factor of eight at s=0.5, and by a factor of four at s=0.8 (see Figure 8-18. Coil currents which were required to support the equilibria are presented in Table 8-13. Each configuration is stable to kink and ballooning modes and was obtained using the free-boundary optimizer.
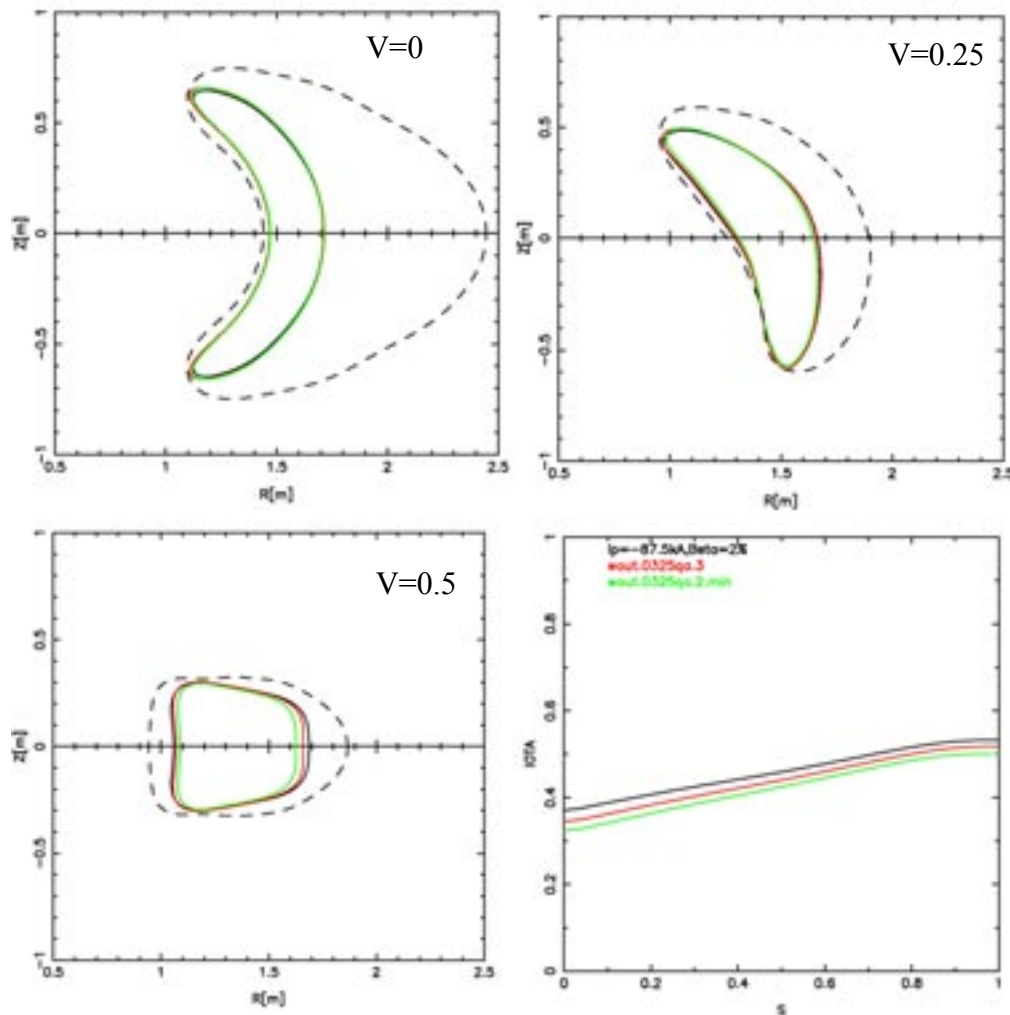
Figure 8-17. Overlay of plasma boundaries for three configurations with $I_p = -87.5$ kA, $\beta = 2.0\%$, the same profiles of plasma current and pressure, but different levels of quasi-axisymmetry (see Table 8-13). Each configuration is stable to kink and ballooning modes
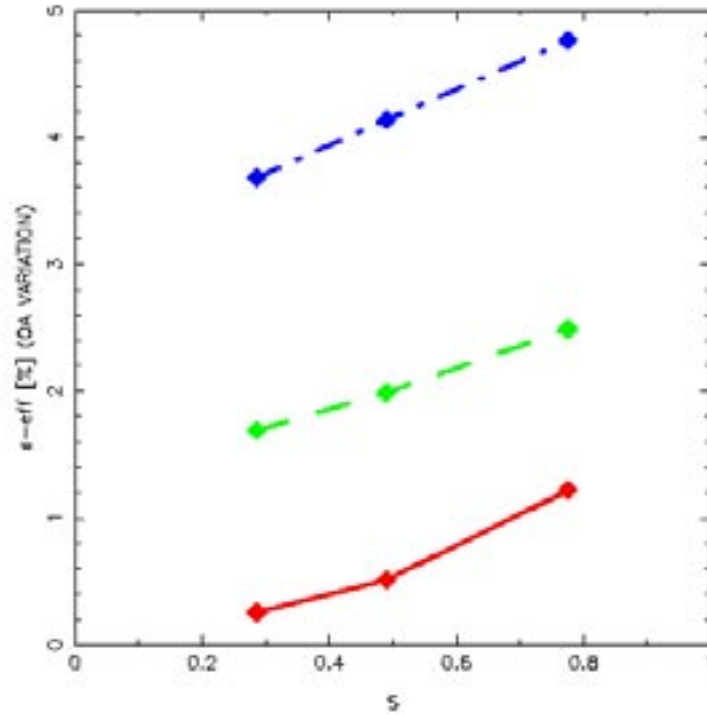
Figure 8-18. Values of ε_{eff} [%] as a function of toroidal flux for three configurations, each with $I_p = -87.5$ kA, $\beta = 2.0\%$, each using the same profiles of plasma current and pressure, and each stable to kink and ballooning modes. The configuration corresponding to the red curve was originally obtained as part of the $I_p - b$ scan discussed in Section 8.3 and presented in Tables 8-4 and 8-5.

ΔI_{M1} [kA-turns]	ΔI_{M2} [kA-turns]	ΔI_{M3} [kA-turns]	ΔI_{TF} [kA-turns]	ΔI_{PF3} [kA-turns]	ΔI_{PF4} [kA-turns]	ΔI_{PF5} [kA-turns]	ΔI_{PF6} [kA-turns]
-111.	-38.	+145.	+0.	+0.	-7.	-2.	+0.

Table 8-13. Difference in coil currents between the blue color coded configuration (high ε_{eff}) shown in Figures 8-17 and 8-18 and the red color coded configuration (optimized ε_{eff} case).

8.8　Summary

We have presented a number of numerical experiments that demonstrate the ability of NCSX coils to meet the NCSX project mission. We have shown

- The NCSX plasma shape/position is robust with respect to uncertainties in the match between plasma profiles and assumed coil currents – e.g., the plasma boundaries displayed in Figure 8-4 were obtained using a variety of assumed plasma profiles and show modest changes in shape/position, whereas Tables 8-7 and 8-9 show the variation in coil currents required for optimized plasmas with different profiles when plasmas are further constrained to be limited by the first wall boundary.

- Using reference S3 plasma profiles there is a wide operating space of I_p, β values for which plasmas supported by NCSX coils are stable to kink and ballooning modes with low helical ripple amplitude ε_h (see Table 8-4).

- NCSX plasma performance is robust with respect to substantial variations in plasma current and pressure profile shape (see Tables 8-7 and 8-9) and the discussion of finite edge current in Section 8.4.2.

- Substantial changes in the external transform $\iota(s)$ and shear $\iota'(s)$ can be induced (see Tables 8-10 and 8-11, and corresponding figures) by varying currents in the NCSX coils. This provides a significant control knob for the experimental determination of stable/unstable operating boundaries and the investigation of 3D shape stabilization.

- NCSX coils have good flexibility to stability boundaries, and to explore the role of 3D shaping in stabilizing MHD modes, see Section 8.6.

- NCSX coils have the flexibility to control the degree of quasi-axisymmetry allowing exploration of the physics of QA plasmas, see Section 8.7.

The extensive flexibility calculations reported in this Chapter have used the un-healed M45 coil system. A subset of these calculations was duplicated using the M45h healed coils. It was found that the M45 coil currents, when used as coil currents in the M45h healed coils, produce essentially identical stable configurations with the same quality of quasi-axisymmetry for states at the corners of flexibility space (the S1, S2 and S3 states in the $I_p - \beta$ scans, and states with $\alpha = 0.5$ in the current profile scans, and $\gamma = 0.8$ in the pressure profile scans). This was to be expected since the healing of resonant fields which led from M45 to M45h required only minor deformations of the M45 coils, and hence minor changes in the equilibrium fields produced by these coils.

Surface quality of non-baseline NCSX plasmas has not been discussed in this Chapter. It was addressed in Chapter 2 with a PIES analysis of various vacuum S1 states, and will be further discussed in Chapter 9 in the analysis of a ramp-up simulation where profile shapes of current

and pressure as well as values of I_p and β vary with time. The PIES analysis of additional states within the operating space of NCSX plasmas is the subject of on-going analysis.

References

[1] D. Mikkelsen, "Standard Profiles for NCSX Flexibility Studies", March 1 2000 http://www.pppl.gov/ncsx/ncsxfss/Physics/physics.html
[2] M.I. Mikhailov, V.D. Shafranov, "Stable Current Profile in a Stellarator with Shear", Nucl. Fusion **30** (1990) 413-421.
[3] R. Jaenicke et al., "Operational Boundaries on the Stellarator W7-AS at the Beginning of the Divertor Experiments", 18th IAEA Fusion Energy Conference, Sorrento, Italy, 4-10 Oct 2000, Paper IAEA-CN-77/OV4/3.